Prediction of viscosity for molecular fluids at experimentally accessible shear rates using the transient time correlation function formalism

Guoai Pan[a] and Clare McCabe[b]
Department of Chemical Engineering, Vanderbilt University, Nashville, Tennessee 37235-1604

(Received 5 June 2006; accepted 27 September 2006; published online 21 November 2006)

Nonequilibrium molecular dynamics (NEMD) simulations were performed and the transient time correlation function (TTCF) method applied to calculate the shear viscosity of *n*-decane. Using the TTCF method we were able to calculate the viscosity at shear rate orders of magnitude lower than is possible by direct NEMD simulation alone. For the first time for a molecular fluid, we were able to simulate shear rates accessible by experimental measurements, which are typically performed at shear rates well below those accessible by NEMD simulation. The TTCF method allows us to close the gap between the lowest shear rates accessible by MD simulation and the highest shear rates possible in experimental studies. Additionally a multiple time step method for Gaussian thermostatted SLLOD equations of motion was developed following earlier work [G. A. Pan *et al.*, J. Chem. Phys. **122**, 4114 (2005)] for atomic fluids. © *2006 American Institute of Physics*.
[DOI: 10.1063/1.2364899]

INTRODUCTION

Over the past two decades molecular dynamics (MD) simulation has emerged as a standard technique with which to study the macroscopic properties of materials. Of particular focus is the use of MD to determine transport properties, as these cannot be easily extracted from a Monte Carlo simulation.[1,2] Molecular simulation methods for calculating viscosity can be broadly classified into equilibrium molecular dynamics (EMD) and nonequilibrium molecular dynamics (NEMD) methods. In an EMD simulation, Newton's equations (or a variant thereof) describing the motion of the atoms in the model system are solved as a function of time. The viscosity η is then given as an integral of the stress-stress autocorrelation functions determined during the simulation, viz.

$$\eta = \frac{V}{k_B T} \lim_{\tau \to \infty} \int_0^\tau dt \langle P_{xy}(t) P_{xy}(0) \rangle, \tag{1}$$

where V is the volume of the system, k_B is Boltzmann's constant, T is the temperature, and t time. The quantity $P_{xy}(t)$ is the value of the xy component of the traceless symmetric stress tensor at time t, and so $P_{xy}(t)P_{xy}(0)$ is the stress-stress autocorrelation function and $\langle P_{xy}(t)P_{xy}(0)\rangle$ is its ensemble average (indicated by $\langle \ldots \rangle$) measured during the course of the simulation. EMD methods based on the application of Eq. (1) (and similar approaches[3]) have been applied routinely and successfully to low molecular weight fluids.[4,5] The success of these methods for such fluids is at least partly the result of the short relaxation times (of the order of 10 ps or less) for the stress-stress autocorrelation function in such systems. The time over which the stress-stress autocorrelation function needs to be computed in order to obtain high-accuracy results from Eq. (1) is at least several hundred relaxation times.[6] As a result, when the relaxation time is of the order of 10 ps or less, the stress-stress autocorrelation function needs to be computed for 10^5–10^6 time steps, since the time step in MD simulations is typically of the order of 10^{-15} s. Hence, EMD simulation may not appear to be a practical approach for long molecules (e.g., alkanes around C_{30} or longer) even with today's computing power. Evidence for this was provided by Cui *et al.* for C_{16}, which represented the simulation limits with the then available computational resources.[4]

While EMD has been used extensively for calculating transport properties, in recent years the NEMD method has become increasingly popular and has been used extensively to predict the rheological properties of real fluids (see, for example, Refs. 7–9 and the references therein). NEMD is a particularly useful technique for studying rheological properties since the key algorithm (SLLOD) (Ref. 10) is a direct implementation of the experimental method for measuring viscosity, and because it can also be used to probe the non-Newtonian regime, common to polymers, and other high-molecular-weight systems. The NEMD SLLOD algorithm for viscosity involves applying a planar Couette flow field at strain rate $\dot{\gamma} = \partial u_x / \partial y$, which characterizes the constant change in streaming velocity u_x in the x direction with vertical position y. These simulations are usually performed in the canonical or isothermal-isobaric ensemble; constant temperature is maintained through the use of well-validated thermostatting methods.[11] The viscosity at strain rate $\dot{\gamma}$ is then computed from

$$\eta = -\frac{\langle P_{xy}^{0,s} \rangle}{\dot{\gamma}}, \tag{2}$$

where $P_{xy}^{0,s}$ is the traceless symmetrized pressure tensor computed during the course of the simulation. The result is a

[a]Present address: Department of Physics, North Dakota State University, ND 58102.
[b]Author to whom correspondence should be addressed. Electronic mail: c.mccabe@vanderbilt.edu

strain-rate dependent shear-thinning viscosity. The critical strain-rate transition $\dot{\gamma}_c$ above which we see shear thinning and below which we see a Newtonian plateau (η independent of $\dot{\gamma}$) typically occurs at $\dot{\gamma}_c \approx \tau^{-1}$, where τ is the longest relaxation time at equilibrium (i.e., in the absence of shear). This is usually the rotational relaxation time (τ_{rot}). In the case of high molecular weight molecules where EMD calculations appear to be infeasible, the NEMD method is the only reliable route to the Newtonian viscosity, albeit computationally expensive. This becomes particularly apparent at high pressures where the rotational relaxation time is of the order of tens of nanoseconds and the shear-thinning regime extends down to very low strain rates.[9]

Since experimental strain rates are limited to around 10^5 s^{-1}, in order to observe non-Newtonian behavior experimentally in a relatively simple fluid (i.e., such as a C_{30} alkane), very high pressures and low temperatures are required because the longest relaxation time of the fluid (τ) must be large enough that the strain rates accessible to experiment will yield non-Newtonian behavior. For a relatively simple fluid this regime will only be reached at very high pressures and low temperatures. As a corollary, for NEMD to reach the Newtonian plateau of the same simple fluid at the same very high pressures and low temperatures, one must simulate strain rates of about 10^5 s^{-1}, over times of the order of multiples of $\tau_{\mathrm{rot}} > 10^{-5}$ s. Thus, it is infeasible with direct simulation to reach the Newtonian plateau, since time scales of this size (10 μs and higher) are inaccessible. Hence prediction of the Newtonian viscosity and direct comparison of experiment and simulation are not possible for such fluids with standard NEMD simulation.

In this work, we have applied the transient time correlation function (TTCF) method, which has been shown to be reliable to low strain rates for model atomic fluids, to predict the shear and Newtonian viscosities of *n*-decane in an effort to make direct contact with experimental studies. As far as the authors are aware, this is the first application of the TTCF method in the prediction of the shear viscosity of a molecular fluid.

METHODS

The transient time correlation function

The TTCF formalism to evaluate shear viscosity was first proposed by Morriss and Evans[11–13] as a generalization of the Green-Kubo relations for nonequilibrium states far from equilibrium. It can be considered a hybrid approach, in that fluctuations in equilibrium microscopic quantities are correlated with the transient response of the system subject to an external force (i.e., under nonequilibrium conditions). The TTCF calculation correlates microquantities of an initial equilibrium state (a local equilibrium state) in the equilibrium trajectory with the corresponding values of these quantities during the establishment of the nonequilibrium state (the transient state). The viscosity is evaluated through the integration of shear stress correlation functions between the local equilibrium state and transient states as given by

$$\langle \eta(t;\dot{\gamma}) \rangle = -\frac{V}{k_B T} \int_0^t ds \langle P_{xy}(s;\dot{\gamma}) P_{xy}(0;\dot{\gamma}=0) \rangle,$$

$$\eta(\dot{\gamma}) = \lim_{t\to\infty} \langle \eta(t;\dot{\gamma}) \rangle. \tag{3}$$

Here $P_{xy}(0;\dot{\gamma}=0)$ is the xy component of the stress tensor at time 0 of the transient process (i.e., a starting configuration from an equilibrium MD simulation), while $P_{xy}(s;\dot{\gamma})$ is the xy component of the stress tensor at time instance s in the transient process at strain rate $\dot{\gamma}$. Therefore, $P_{xy}(s;\dot{\gamma})P_{xy}(0;\dot{\gamma}=0)$ is the correlation function of stress in a local equilibrium state with that of a transient state at time s, and $\langle P_{xy}(s;\dot{\gamma})P_{xy}(0;\dot{\gamma}=0)\rangle$ its ensemble average. The shear viscosity at shear rate $\dot{\gamma}$ is the integral of the correlation function over infinite time.

Borzsák *et al.*[14] have applied the TTCF formalism to calculate the shear viscosity of a Weeks-Chandler-Anderson (WCA) fluid over a wide range of shear rates (in reduced units from $\gamma = 1.0^{-7} - 1.0$), expanding on the initial work of Morriss and Evans.[11–13] The TTCF calculations successfully determined the viscosities at low shear rates, beyond the range in which NEMD simulations can be used due to poor signal to noise ratio, and predicted consistent results with NEMD at higher shear rates. In a similar approach, Delhommelle and Cummings[15] have studied the shear viscosity of a WCA fluid in a confined geometry to low shear rates.

Algorithm

Molecular dynamics simulations were performed in the isothermal-isochoric ensemble. The application of a thermostat in the transient stage of the TTCF calculation was a key factor of Morriss and Evans'[12] success, compared to the earlier work of Dufty and Lindenfeld,[16] in which no steady state could be reached and the transient correlation function diverged. In this work in order to maintain constant temperature a Gaussian thermostat[17] is used; therefore the average kinetic energy per particle is held rigorously constant while generating the correct canonical ensemble averages for all properties that depend only on the positions of the particles.[1,11,17,18] This choice is motivated by the fact that the Gaussian thermostat is "self-starting," i.e., it does not require an empirical relaxation time for temperature control, which is an important property for the transient NEMD simulations performed in the TTCF method. The SSLOD equations[11] of motion for particle i in planar Couette flow with Lees-Edwards boundary conditions are given by

$$\frac{d\mathbf{r}_i}{dt} = \frac{\mathbf{p}_i}{m_i} + \dot{\gamma} y_i \hat{\mathbf{x}},$$

$$\frac{d\mathbf{p}_i}{dt} = \mathbf{F}_i - \dot{\gamma} p_{y,i} \hat{\mathbf{x}} - \alpha \mathbf{p}_i, \tag{4}$$

where $\mathbf{r} = (x, y, z)$ and $\mathbf{p} = (p_x, p_y, p_z)$ are the particle positions and momentum, $\dot{\gamma}$ is the shear rate, d_x is the lattice strain under Lees-Edwards periodic boundary conditions, $\hat{\mathbf{x}}$ is a unit vector in the x direction, and $\mathbf{F}_i$ the force acting on

particle i. In the momentum equation of motion, the Gaussian thermostat multiplier α (or "friction coefficient") is applied to conserve the kinetic energy of the system, $d/dt\Sigma_i \mathbf{p}_i^2/2m_i=0$, which leads to the variable α at each time step:

$$\alpha = \frac{\sum_i (\mathbf{F}_i \cdot (\mathbf{p}_i/m_i) - \dot{\gamma} p_{x,i} p_{y,i}/m_i)}{\sum_i \mathbf{p}_i^2/m_i}. \quad (5)$$

Since α depends on both the forces and moment of the particles, kinetic energy drift is observed when a conventional integrator is used to integrate the Gaussian thermostatted SLLOD equations. Note that these equations of motion imply an atomic thermostat. Such a thermostat is not rigorously correct, as shown by Travis *et al.*[19,20] This is because a molecular fluid in a shear field undergoes shear-induced rotational motion that should be subtracted from the rotational velocity to determine the peculiar rotation motion that can then be thermostatted. Applying an atomic thermostat, as given above, does not in principle achieve this goal. As shown by Lue *et al.*,[21] one can instead thermostat only the center-of-mass motion, leading to more complicated equations of motion. However, differences in viscosity between rigorously thermostatted systems and the atomic thermostat (as used in this work) are evident only in the nonlinear response regime. For rigid diatomics (i.e., chlorine), for example, Travis *et al.*[20] saw a difference between atomic and rigorously thermostatted systems at reduced strain rates of approximately 2 and higher. All of the TTCF simulation results presented in this paper are at extremely low strain rates (between 5×10^{-7} and 4×10^{-2} in reduced units) and hence at least two orders of magnitude below any strain rate at which complications due to the approximate nature of the thermostat could be expected. For this reason, we do not believe the TTCF results are in any way impacted by our choice of thermostat.

In previous work, based on earlier work by Zhang,[22] a homogeneous algorithm for simulating atomic fluids using the Gaussian thermostatted equations of motion for both equilibrium and SLLOD nonequilibrium dynamics was developed. The new algorithm ensures the conservation of kinetic energy at each time step and therefore eliminates any temperature drift.[23] This is achieved by splitting the extended system Liouville operator into position (**A**) and momentum (**B**) vectors and deriving analytical solutions for the resulting equations. Due to the coupling of the shear rate and forces in the Gaussian thermostat multiplier a further split on vector **B** is needed to derive an analytic solution. Using Gauss' principle of least constraint to ensure kinetic energy conservation in each substep of integration, **B** is split into **B**1 for the equations containing the shear field and **B**2 for the equations containing the forces. The Gaussian thermostatted operator splitting algorithm has been shown to exhibit extreme stability in temperature control and allow larger simulation time steps.[23]

In order to apply the operator-splitting algorithm to molecular fluids in which motions occur on different time scales, (i.e., the internal motions of the atoms occur on a faster time scale than the intermolecular interactions) we have developed, and present here for the first time, a multiple time step method for the SLLOD equations of motion coupled with a Gaussian thermostat and the operator-splitting algorithm to achieve strict kinetic energy control (a derivation of the algorithm is provided in the Appendix). This is achieved by combining the operator-splitting algorithm with the reversible reference system propagator algorithm (rRESPA) developed for multiple time scales of motion by Tuckerman *et al.*[24] rRESPA has been successfully used in the simulation of atomistically detailed complex fluids (see, for example, Refs. 8, 9, and 25–27). In particular, Cui *et al.*[27] developed a multiple time step method for the atomic SLLOD equations of motion coupled with a Nosé-Hoover thermostat. We will compare results obtained from the algorithm used in this work with those from Cui *et al.*[27] in order to validate the proposed method before using it in the TTCF calculations.

Models and simulation details

We have performed MD simulations of *n*-decane using the Siepmann-Karaborni-Smit (SKS) united atom (UA) model proposed by Siepmann *et al.*[28] for the prediction of phase equilibria of *n*-alkanes. As in earlier work,[27] we use the modification of Mundy *et al.*[26] in which the fixed bond length is replaced by a stiff harmonic potential to generate a fully flexible model. We will briefly describe the model; the reader is referred to the original papers for full details.

In the UA model, the CH_3 and CH_2 groups are coarse grained into single spherical interaction sites with the interaction center located at the center of each carbon atom. A Lennard-Jones potential describes the intermolecular interactions and the intramolecular interactions between sites separated by three or more bonds. Simple Lorentz-Berthelot combining rules were used to determine the cross or unlike interactions and a cutoff distance of $2.5\sigma_0$, (9.825 Å) was used, where $\sigma_0=3.93$ Å and corresponds to the diameter of the CH_2 united atom site. Bond stretching and bond angle bending are described by harmonic potentials. The potential of Jorgensen *et al.*[29] is used to determine the torsional motion characterizing the preferred orientational and rotational barriers around all nonterminal bonds.

Simulations were carried out on 100 *n*-decane molecules at 480 K and a density of 0.6136 g/cm^3. This state point was chosen in order to compare with the work of Cui *et al.*[27] and Mundy *et al.*[30] who studied the viscosity of *n*-decane through EMD and NEMD simulations. A time step size of 2.35 fs was used for slow motions and a sub-time-step-size of 0.235 fs for the fast motions in the multiple time step method. Note that using the characteristic energy and length scales of a CH_2 group, one unit of dimensionless time, equal to $\sqrt{m\sigma^2/\varepsilon}$, is 2.35 ps. Hence these time steps correspond to 10^{-3} and 10^{-4} in dimensionless time units.

During the simulations the pressure tensor **P** can be calculated through the atomic formalism in which the sum in Eq. (6) is over all atoms,

$$\mathbf{P}^{(a)}V = \sum_{ia} \left(\frac{\mathbf{p}_{ia}\mathbf{p}_{ia}}{m_{ia}} + \mathbf{r}_{ia}\mathbf{F}_{ia} \right), \tag{6}$$

where m_{ia} is the mass of atom ia, $\mathbf{r}_{ia}$ and $\mathbf{p}_{ia}$ are the coordinates and momentum of atom ia, and $\mathbf{F}_{ia}$ is the sum of all the forces acting on atom ia. Alternatively the molecular formalism can be used, in which the summation is over all molecules,

$$\mathbf{P}^{(m)}V = \sum_{i} \left(\frac{\mathbf{p}_{i}\mathbf{p}_{i}}{m_{i}} + \mathbf{r}_{i}\mathbf{F}_{i} \right). \tag{7}$$

Here m_i is the mass of molecule i, $\mathbf{r}_i$ and $\mathbf{p}_i$ are coordinates and momentum of the center of mass of molecule i, and $\mathbf{F}_i$ is the sum of all intermolecular forces acting on any interaction sites of molecule i. While we use both formalisms in the NEMD simulations reported in this work we use the atomic formalism in the TTCF calculations presented.

RESULTS

In order to validate the multiple time step method for Gaussian thermostatted SLLOD equations of motion, both EMD and NEMD simulations were performed and compared with simulations using the Nosé-Hoover thermostat. In the EMD simulations, the viscosity is calculated through the Green-Kubo relation in Eq. (1). The equilibration of the system was carried out following Cui *et al.*[27] The molecules were placed in the simulation box with their center of mass at lattice points in the all *trans* conformation. The Lennard-Jones (LJ) interaction was grown from $0.05\sigma_0$ to σ_0 in a 20 000 time step initialization period during which rescaling of the velocities was performed. Velocity rescaling was continued for a further 110 000 time steps, followed by an additional 4.2×10^5 time steps ($\sim$1 ns) of thermostatted equilibration. Production runs were performed for 5×10^6 time steps ($\sim$10 ns) starting from the aforementioned equilibrated configurations. The viscosities obtained by Green-Kubo integration with the Gaussian and Nosé-Hoover thermostat, with three different Nosé time constants, using the atomic shear stress correlation functions are shown in Fig. 1. The viscosities with Nosé time constants of $\tau=0.15$ ps, $\tau=0.3$ ps, and $\tau=0.62$ ps were determined to be 0.175 ± 0.004 cP, 0.181 ± 0.003 cP, and 0.179 ± 0.005 cP, respectively. The viscosity from the simulation performed with the Gaussian thermostat is 0.174 ± 0.003 cP. Given that the values for the viscosity from all four simulations are within statistical uncertainty, the calculations are in agreement.

We have also performed NEMD simulations with the Gaussian and Nosé-Hoover thermostats, with a Nosé time constant of $\tau=0.3$ ps. The shear stress was calculated using both the atomic and molecular formalisms and the viscosity evaluated as in Eq. (3). The results are given in Table I and plotted in Fig. 2. From these, and the EMD simulations, we can conclude that the multiple time step method developed for the Gaussian thermostatted SLLOD equations of motion generates results for the viscosity of *n*-decane that are consistent with those from Cui *et al.*[27] using the Nosé-Hoover thermostat and rRESPA algorithm.

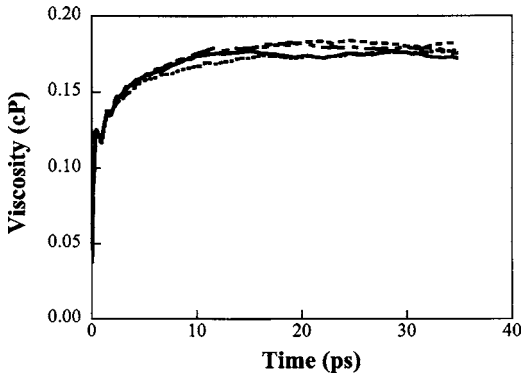

FIG. 1. Viscosities for *n* decane predicted from the Green-Kubo formalism using the atomic shear stress autocorrelation function and the Gaussian (solid line) or Nosé thermostats with time constants $\tau=0.15$ ps (dotted line), $\tau=0.3$ ps (short dashed line), and $\tau=0.62$ ps (long dashed line).

Having validated the Gaussian thermostatted SLLOD equations of motions, we can now apply this method to TTCF calculations. Simulations were carried out in the low shear regime, i.e., below $\dot{\gamma}=0.04$ $(1.7\times10^{10}\ \mathrm{s}^{-1})$ which is the lowest shear rate in the NEMD simulations for which we were able to get a reasonable signal/noise ratio. The transient processes were started from independent configurations taken from EMD Gaussian thermostatted simulations described previously for the Green-Kubo calculations of viscosity. Configurations were saved every 500 time steps, in order to obtain relatively uncorrelated configurations from which to start the TTCF calculations. In each transient calculation, starting from an initial equilibrated configuration, the shear field is turned on and the simulation run for a given length of time, which should be greater than the characteristic time required for the system to relax to a steady state. During the transient stage (i.e., starting with the equilibrium configuration to the attainment of steady state under shear),

TABLE I. Predicted viscosities from NEMD simulations of *n*-decane using the Gaussian thermostat and the Nosé-Hoover thermostat with Nosé time constant $\tau=0.3$ ps. Results obtained from both the atomic stress and molecular stress formalisms are reported.

Reduced shear rates	Shear rates (s^{-1})	Atomic stress formalism η (cP)	Molecular stress formalism η (cP)
	Gaussian thermostat		
0.04	1.70×10^{10}	0.184±0.009	0.181±0.009
0.09	3.83×10^{10}	0.182±0.006	0.179±0.005
0.16	6.81×10^{10}	0.181±0.004	0.178±0.004
0.36	1.53×10^{11}	0.167±0.003	0.164±0.002
0.64	2.72×10^{11}	0.152±0.002	0.148±0.002
1.00	4.26×10^{11}	0.143±0.002	0.138±0.002
1.44	6.13×10^{11}	0.137±0.001	0.132±0.001
	Nosé-Hoover thermostat		
0.04	1.70×10^{10}	0.182±0.009	0.179±0.009
0.09	3.83×10^{10}	0.184±0.007	0.181±0.007
0.16	6.81×10^{10}	0.177±0.003	0.175±0.003
0.36	1.53×10^{11}	0.164±0.002	0.160±0.001
0.64	2.72×10^{11}	0.155±0.002	0.151±0.002
1.00	4.26×10^{11}	0.143±0.002	0.139±0.002
1.44	6.13×10^{11}	0.135±0.001	0.131±0.001

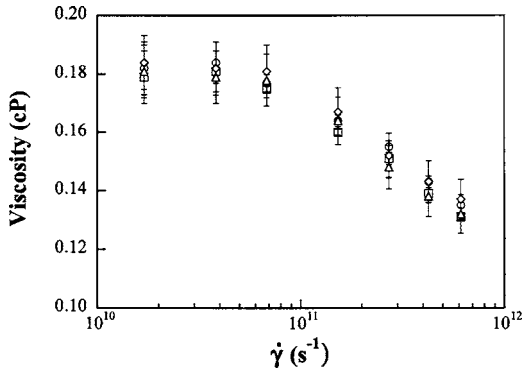

FIG. 2. Strain-rate dependent viscosities for *n* decane predicted from NEMD simulations using the Gaussian thermostat, with the atomic (diamonds) and molecular (triangles) shear stress autocorrelation functions, and the Nosé thermostat (with time constant τ=0.3 ps), with the atomic (circles) and molecular (squares) shear stress autocorrelation functions.

the shear stress is correlated with the shear stress at the starting configuration, as described earlier. The correlation function is averaged over repeated transient processes from different, independent, starting configurations and the viscosity evaluated through Eq. (3). This is achieved through trajectory mapping,[11,12] which is a central part of the TTCF calculation. A pair of reflections in a coordinate or momentum axis on the starting configurations will lead to four new starting configurations making pairs of phase space of Γ_i and $-\Gamma_i$, which have the same occurring probability within the equilibrium distribution of states. This results in the sum of shear stresses $P_{xy}(\Gamma)$ from these four starting configurations being zero and helps to minimize the statistical uncertainties in the TTCF integral of viscosity because at long time the correlation function in Eq. (3) becomes $\sim\langle P_{xy}(\infty)\rangle\langle P_{xy}(0)\rangle$. The trajectory mapping technique eliminates the statistical difficulties associated with the small, yet nonzero, value of $\langle P_{xy}(0)\rangle$ at long times.

In the work of Borzák *et al.*[14] on the WCA fluid, the TTCF was averaged over $4\times 30\,000$ configurations (where 4 indicates the four new starting configurations derived from the trajectory mapping technique), with 600 time steps in the transient process. Since, *n*-decane has a much longer relaxation time ($\sim$10 ps at the current state point[31]) than the WCA model fluid, it requires longer correlation times for the TTCF calculations. We performed simulations at five different shear rates using the following number of time steps for the transient period; 7000 time steps (16.45 ps) were used for $\dot{\gamma}=0.04(1.7\times 10^{10}\ s^{-1})$ and $\dot{\gamma}=5\times 10^{-4}(2.13\times 10^{8}\ s^{-1})$ and 10 000 time steps (23.5 ps) were used for the lower shear rates, $\dot{\gamma}=5\times 10^{-5}(2.13\times 10^{7}\ s^{-1})$, $\dot{\gamma}=5\times 10^{-6}(2.13\times 10^{6}\ s^{-1})$, and $\dot{\gamma}=5\times 10^{-7}(2.13\times 10^{5}\ s^{-1})$. These correlation times are longer than the longest relaxation time of *n*-decane, i.e., the molecular orientation relaxation time. We averaged over $4\times 18\,000$–$4\times 30\,000$ starting configurations in order to get convergent TTCF viscosities. While this involves a large amount of simulation time (1.2×10^{9} time steps were performed for the longest simulation), the TTCF calculation can be efficiently parallelized as long as a pool of starting configurations from an EMD simulation are available. With such a configuration pool, TTCF simulations at various shear rates can be performed on each processor in a "perfectly parallel" or "embarrassingly parallel" fashion.[32]

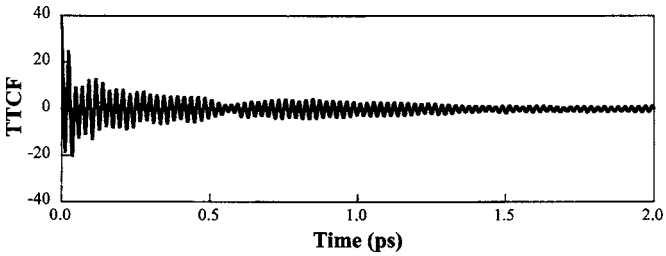

FIG. 3. Transient time correlation function of atomic shear stress at a reduced shear rate of 0.0005.

The TTCF calculations were performed with correlation functions for the atomic shear stress and as can be seen from Fig. 3 exhibit strong oscillatory behavior. We note that the period of the oscillation is 0.023 ps, which is a fraction (10^{-2}) of the characteristic time unit in the UA model[31] (2.35 ps) and corresponds to the harmonic bond stretching.[31] This illustrates the need to carefully select the time intervals at which to evaluate atomic stress correlation functions, in order to avoid missing the true oscillatory behavior, and can lead to inaccurate values for the viscosity. The strong oscillation in the atomic shear stress transient time correlation functions is also reflected in the oscillatory nature of the integral viscosity curve, as seen in Fig. 4. The viscosities from the atomic shear stress TTCF integrals are reported in Table II and plotted with the viscosities obtained from the direct NEMD simulations in Fig. 5. As can be seen from the figure, the data are fitted well by the Cross model,[33] which is used to describe the shear-thinning behavior of polymeric fluids:

$$\eta(\dot{\gamma}) = \eta_\infty + \frac{\eta_0 - \eta_\infty}{1 + (a\cdot\dot{\gamma})^n}, \tag{8}$$

where, if $\dot{\gamma}$ is in real units of s^{-1}, the fitting parameters are η_0=0.182, η_∞=0.134, $a=4.41\times 10^{-11}$ s, and n=2.48. The fit suggests a Newtonian plateau at very low shear rates, with a zero shear viscosity of 0.182 cP, followed by a shear-thinning region. We note that Fig. 5 presents viscosities for *n*-decane over six orders of magnitude in shear rate and that the lowest shear rate of 10^{-5} s^{-1} in the TTCF simulations brings the simulations into the range of experimentally accessible shear rates.

TABLE II. Viscosities of *n*-decane predicted from TTCF calculations at various shear rates.

Reduced shear rate	Shear rate (s^{-1})	Atomic viscosity (cP)
0.000 000 5	2.13×10^{5}	0.182±0.007
0.000 005	2.13×10^{6}	0.176±0.014
0.000 05	2.13×10^{7}	0.186±0.008
0.000 5	2.13×10^{8}	0.182±0.009
0.04	1.70×10^{10}	0.178±0.013

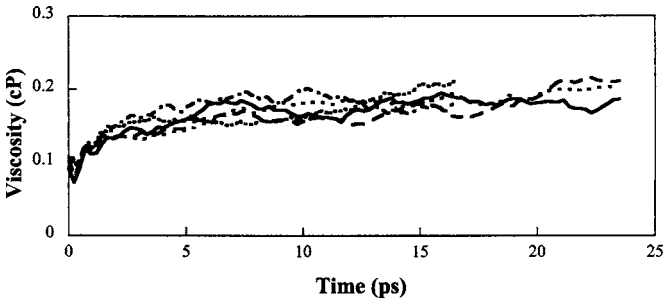

FIG. 4. Viscosities from TTCF calculations using the atomic shear stress correlation function at various shear rates. The curves are for different shear rates $\dot{\gamma}$ applied in transient states: solid line $\dot{\gamma}=5\times10^{-7}$; long dashed line $\dot{\gamma}=5\times10^{-6}$; short dashed line $\dot{\gamma}=5\times10^{-5}$; dash dotted dashed line $\dot{\gamma}=5\times10^{-4}$; dotted line $\dot{\gamma}=4\times10^{-2}$.

CONCLUSIONS

We have developed a multiple time step method for MD simulations using the Gaussian thermostatted SLLOD equations of motion. The method combines the operator-splitting technique with rRESPA to strictly control the kinetic energy in the integration steps of multiatomic molecules. The conservation of kinetic energy is completely independent of the systems historic information, which makes it a natural choice for the TTCF calculation, where initialization of the nonequilibrium, transient states is required without using information from previous time steps. A comparison of viscosities from EMD and NEMD simulations using the Nosé-Hoover thermostat and the Gaussian thermostat was performed to validate the developed multiple time step method. We find that the viscosities calculated from the atomic and molecular formalisms agree in Green-Kubo EMD calculations and NEMD simulations, which is consistent with the literature.[6,31,34]

The TTCF method has been shown to successfully predict the Newtonian plateau and shear flow viscosity for *n*-decane. We have demonstrated that TTCF can be used to determine the viscosity of molecular fluids at shear rates beyond those accessible by direct NEMD simulation, due to the poor signal of the nonequilibrium response compared to the noise from equilibrium fluctuations. The TTCF method can therefore be used to bridge the gap between NEMD and Green-Kubo calculations. At the lowest shear rates studied, 10^5 s^{-1}, we have moved molecular simulation into a regime where direct contact with experiment is possible. TTCF is therefore able to probe the transport properties of systems in which shear thinning occurs at shear rates lower than those reachable by NEMD but higher than the experimental range.

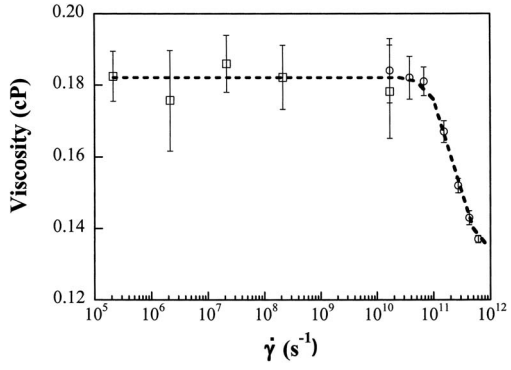

FIG. 5. The viscosities of *n* decane calculated over a wide range of shear rates. The squares represent viscosities from the TTCF calculations using the atomic shear stress correlation and the circles represent the viscosities from the atomic shear stress calculation of NEMD simulations. The dashed line is a fit to the Cross model.

ACKNOWLEDGMENTS

The authors would like to thank István Borzsák, Denis Evans, and Peter Cummings for useful discussions. They also acknowledge the American Chemical Society Petroleum Research Fund for financial support and the Center for Computational Sciences at Oak Ridge National Laboratory and the National Energy Research Scientific Computing Center for computational resources. One of the authors (G.P.) would also like to thank Daniel Kroll for encouragement and partial support from the National Science Foundation under Grant No. DMR-0513393 and ND EPSCoR through NSF Grant No. EPS-0132289, during the writing stages of this work.

APPENDIX: DERIVATION OF THE MULTIPLE TIME STEP OPERATOR-SPLITTING ALGORITHM

Here we present the operator-splitting multiple time step method for Gaussian thermostatted SLLOD equations of motion developed in this work.

The phase variable Liouville operator for Gaussian thermostatted SLLOD equations of motions [Eq. (4)] is given by

$$iL=\sum_i \dot{\mathbf{r}}_i\cdot\frac{\partial}{\partial\mathbf{r}_i}+\sum_i \dot{\mathbf{p}}_i\cdot\frac{\partial}{\partial\mathbf{p}_i}+\dot{\gamma}\cdot\frac{\partial}{\partial d_x}$$
$$=\sum_i \frac{\mathbf{p}_i}{m_i}\cdot\frac{\partial}{\partial\dot{\mathbf{r}}_i}+\dot{\gamma}\sum_i y_i\cdot\frac{\partial}{\partial x_i}+\sum_i \mathbf{F}_i\cdot\frac{\partial}{\partial\mathbf{p}_i}$$
$$-\dot{\gamma}\sum_i p_{y_i}\cdot\frac{\partial}{\partial p_{x_i}}-\alpha\sum_i \mathbf{p}_i\cdot\frac{\partial}{\partial\mathbf{p}_i}+\dot{\gamma}\cdot\frac{\partial}{\partial d_x}. \tag{A1}$$

The Liouvillean can be decomposed into different components according to the rRESPA multiple time step algorithm depending on the different time scales. For *n* alkanes, motions can be classified into two categories: fast motions, due to the intramolecular interactions, and slow motions, due to the translational motions and intermolecular interactions. Thus the chosen reference system Liouvillean for the fast motions becomes

$$iL_r=\sum_i \frac{\mathbf{p}_i}{m_i}\cdot\frac{\partial}{\partial\dot{\mathbf{r}}_i}+\sum_i \mathbf{F}_{ri}\cdot\frac{\partial}{\partial\mathbf{p}_i}+\alpha_F\sum_i \mathbf{p}_i\cdot\frac{\partial}{\partial\mathbf{p}_i}, \tag{A2}$$

where $\mathbf{F}_{ri}$ is sum of all the forces acting on atom *i* except for the intermolecular forces and α_F is the Gaussian thermostat multiplier corresponding to the force $\mathbf{F}_{ri}$ applied to conserve the kinetic energy in this step,

$$\alpha_F=\frac{\sum_i \mathbf{F}_{ri}\cdot\mathbf{p}_i/m_i}{\sum_i \mathbf{p}_i^2/m_i}. \tag{A3}$$

The Liouvillean for slow motions, $i\Delta L=iL-iL$, is given by

$$i\Delta L = \dot{\gamma}\sum_i y_i \cdot \frac{\partial}{\partial x_i} + \sum_i \mathbf{f}_i \cdot \frac{\partial}{\partial \mathbf{p}_i} - \dot{\gamma}\sum_i p_{y_i} \cdot \frac{\partial}{\partial p_{x_i}} - \alpha_f \sum_i \mathbf{p}_i \cdot \frac{\partial}{\partial \mathbf{p}_i}, \tag{A4}$$

where $\mathbf{f}_i$ includes all the intermolecular forces acting on atom i and α_f is the Gaussian thermostat multiplier

$$\alpha_f = \frac{\sum_i \mathbf{f}_i \cdot \mathbf{p}_i/m_i - \hat{x}\dot{\gamma}p_{xi}p_{yi}/m_i}{\sum_i \mathbf{p}_i^2/m_i}. \tag{A5}$$

Using the operator-splitting algorithm, the reference system Liouvillean can be solved by the time propagator:

$$\exp(iL_r/\Delta t) = \left\{\exp\left[\frac{\delta t}{2}A_r \cdot \frac{\partial}{\partial \Gamma}\right]\exp\left[\delta t B_r \cdot \frac{\partial}{\partial \Gamma}\right] \times \exp\left[\frac{\delta t}{2}A_r \cdot \frac{\partial}{\partial \Gamma}\right]\right\}^n, \tag{A6}$$

where the integration time step Δt is divided into n steps of smaller time step δt for the reference system. The operators with A_r and B_r in Eq. (A6) correspond to integrating over the two vectors in Eqs. (A7) and (A8), respectively,

$$\frac{\partial}{\partial t}\mathbf{r}_i = \frac{\mathbf{p}_i}{m_i}, \quad \frac{\partial}{\partial t}\mathbf{p}_i = 0, \tag{A7}$$

$$\frac{\partial}{\partial t}\mathbf{r}_i = 0, \quad \frac{\partial}{\partial t}\mathbf{p}_i = \mathbf{F}_{ri} - \alpha_F \mathbf{p}_i. \tag{A8}$$

The analytical solution for the A_r operator is given by

$$\mathbf{r}_i(t+\delta t) = \mathbf{r}_i(t) + \delta t \cdot \frac{\mathbf{p}_i(t)}{m_i}, \qquad \mathbf{p}_i(t+\delta t) = \mathbf{p}_i(t). \tag{A9}$$

The analytical solution for the B_r operator is given by

$$\mathbf{r}_i(t+\delta t) = \mathbf{r}_i(t), \qquad \mathbf{p}_i(t+\delta t) = \frac{1-h}{f(\delta t) - h/f(\delta t)}\left[\mathbf{p}_i(t) - \mathbf{F}_{ri}(t) \times \frac{1+h-f(\delta t)-h/f(\delta t)}{(1-h)\beta}\right], \tag{A10}$$

with the following definitions:

$$\beta = \sqrt{\frac{\sum_i \mathbf{F}_{ri}(t)\cdot\mathbf{F}_{ri}(t)/m_i}{\sum_i \mathbf{p}_i^2(t)/m_i}}, \tag{A11}$$

$$f(\delta t) = \exp(-\beta \delta t), \tag{A12}$$

$$\alpha(0) = \frac{\sum_i \mathbf{F}_{ri}(t)\cdot\mathbf{p}_i(t)/m_i}{\sum_i \mathbf{p}_i^2(t)/m_i}, \tag{A13}$$

$$h = \frac{\alpha(0)+\beta}{\alpha(0)-\beta}. \tag{A14}$$

Through second order Trotter factorization, the time propagator solving the phase variable Liouville operator in Eq. (A1) is given as

$$\begin{aligned} U(\Delta t) &= \exp[(i\Delta L + iL_r)\Delta t] \\ &= \exp\left(\frac{\Delta t}{2}B_2\frac{\partial}{\partial\Gamma}\right)\exp\left(\frac{\Delta t}{2}B_1\frac{\partial}{\partial\Gamma}\right)\exp\left(\frac{\Delta t}{2}A\frac{\partial}{\partial\Gamma}\right)\exp(iL_r\Delta t)\exp\left(\frac{\Delta t}{2}A\frac{\partial}{\partial\Gamma}\right)\exp\left(\frac{\Delta t}{2}B_1\frac{\partial}{\partial\Gamma}\right)\exp\left(\frac{\Delta t}{2}B_2\frac{\partial}{\partial\Gamma}\right) \\ &= \exp\left(\frac{\Delta t}{2}B_2\frac{\partial}{\partial\Gamma}\right)\exp\left(\frac{\Delta t}{2}B_1\frac{\partial}{\partial\Gamma}\right)\exp\left(\frac{\Delta t}{2}A\frac{\partial}{\partial\Gamma}\right)\left\{\exp\left[\frac{\delta t}{2}A_r\frac{\partial}{\partial\Gamma}\right]\exp\left[\delta t B_r\frac{\partial}{\partial\Gamma}\right]\exp\left[\frac{\delta t}{2}A_r\frac{\partial}{\partial\Gamma}\right]\right\}^n \\ &\quad \times \exp\left(\frac{\Delta t}{2}A\frac{\partial}{\partial\Gamma}\right)\exp\left(\frac{\Delta t}{2}B_1\frac{\partial}{\partial\Gamma}\right)\exp\left(\frac{\Delta t}{2}B_2\frac{\partial}{\partial\Gamma}\right). \end{aligned} \tag{A15}$$

Here the operators of A, B_1, and B_2 are components related to the slow motion. The operator of A, given in Eq. (A16), is the component that involves the coordinate vector and lattice strain, and Eq. (A17) gives the associated analytical solution.

$$\frac{\partial}{\partial t}\mathbf{r}_i = \dot{\gamma} y_i \hat{x}, \quad \frac{\partial}{\partial t}\mathbf{p}_i = 0, \quad \frac{d}{dt} d_x = \dot{\gamma}, \tag{A16}$$

$$\begin{aligned} x_i(t+\Delta t) &= x_i(t) + \Delta t \dot{\gamma} y_i(0), \\ y_i(t+\Delta t) &= y_i(t), \\ z_i(t+\Delta t) &= z_i(t), \\ d_x(t+\Delta t) &= d_x(t) + \Delta t \dot{\gamma}, \\ \mathbf{p}_i(t+\Delta t) &= \mathbf{p}_i(t). \end{aligned} \tag{A17}$$

The operator of B_1, given in Eq. (A18), is the slow motion component involving the external flow field. The Gaussian thermostat is applied through α_{f1} to conserve kinetic energy in this step. Equation (A20) gives the analytical solution to Eq. (A18).

$$\frac{\partial}{\partial t}\mathbf{r}_i = 0,$$

$$\frac{\partial}{\partial t}\mathbf{p}_i = -\dot{\gamma} p_{y,i} \hat{x} - \alpha_{f1}\mathbf{p}_i, \tag{A18}$$

$$\frac{d}{dt} d_x = 0,$$

$$\alpha_{f1} = \frac{-\sum_i \dot{\gamma} p_{xi} p_{yi}/m_i}{\sum_i \mathbf{p}_i^2/m_i}, \tag{A19}$$

$$\begin{aligned} \mathbf{r}_i(t+\Delta t) &= \mathbf{r}_i(t), \\ \mathbf{p}_i(t+\Delta t) &= g(\Delta t)[\mathbf{p}_i(t) - \hat{x}\Delta t \dot{\gamma} p_{yi}(t)], \\ d_x(t+\Delta t) &= d_x(t). \end{aligned} \tag{A20}$$

In Eq. (20), the function $g(\Delta t)$ is defined as

$$g(\Delta t) = \frac{1}{\sqrt{1 - 2c_1\Delta t + c_2 \Delta t^2}}, \tag{A21}$$

with c_1 and c_2 given by

$$c_1 = \frac{\dot{\gamma}}{\sum_i \mathbf{p}_i^2/m_i} \sum_i p_{xi}(t) p_{yi}(t)/m_i, \tag{A22}$$

$$c_2 = \frac{\dot{\gamma}^2}{\sum_i \mathbf{p}_i^2/m_i} \sum_i p_{yi}(t) p_{yi}(t)/m_i. \tag{A23}$$

The operator of B_2 given in Eq. (A24) is the slow motion component involving only intermolecular interactions. The Gaussian thermostat is applied through α_{f2} to conserve kinetic energy in this step. Equation (A26) provides the analytical solution to Eq. (A24).

$$\frac{\partial}{\partial t}\mathbf{r}_i = 0, \quad \frac{\partial}{\partial t}\mathbf{p}_i = \mathbf{F}_i - \alpha_{f2}\mathbf{p}_i, \quad \frac{d}{dt} d_x = 0, \tag{A24}$$

$$\alpha_{f2} = \frac{\sum_i \mathbf{f}_i \cdot \mathbf{p}_i/m_i}{\sum_i \mathbf{p}_i^2/m_i}, \tag{A25}$$

$$\begin{aligned} \mathbf{r}_i(t+\Delta t) &= \mathbf{r}_i(t), \\ \mathbf{p}_i(t+\Delta t) &= \frac{1-h}{f(\Delta t) - h/f(\Delta t)} \Bigg[\mathbf{p}_i(t) \\ &\quad - \mathbf{f}_i(t) \frac{1 + h - f(\Delta t) - h/f(\Delta t)}{(1-h)\beta} \Bigg], \\ d_x(t+\Delta t) &= d_x(t), \end{aligned} \tag{A26}$$

where

$$\beta = \sqrt{\frac{\sum_i \mathbf{f}_i \cdot \mathbf{f}_i/m_i}{\sum_i \mathbf{p}_i^2/m_i}}, \tag{A27}$$

$$h = \frac{\alpha(0) + \beta}{\alpha(0) - \beta}, \tag{A28}$$

$$f(\Delta t) = \exp(-\beta \Delta t). \tag{A29}$$

The function $\alpha(0)$ in Eq. (A28) is defined as

$$\alpha(0) = \frac{\sum_i \mathbf{f}_i \cdot \mathbf{p}_i/m_i}{\sum_i \mathbf{p}_i^2/m_i}. \tag{A30}$$

The Gaussian thermostat is applied in the equations of momenta, Eqs. (A8), (A18), and (A24), which ensures the kinetic energy conservation in the time propagator presented in Eq. (A15), while the analytical solutions provided for all the operators in Eq. (A15) guarantee the numerical stability of the algorithm.

[1] M. P. Allen and D. J. Tildesley, *Computer Simulation of Liquids* (Oxford University Press, Oxford, 1987).
[2] B. Hess, J. Chem. Phys. **116**, 209 (2002).
[3] P. J. Daivis and D. J. Evans, J. Chem. Phys. **100**, 541 (1994).
[4] S. T. Cui, P. T. Cummings, and H. D. Cochran, Mol. Phys. **93**, 117 (1998).
[5] J. M. Haile, *Molecular Dynamics Simulation* (Wiley, New York, 1992); M. Mondello and G. S. Grest, J. Chem. Phys. **103**, 7156 (1995).
[6] M. Mondello and G. S. Grest, J. Chem. Phys. **106**, 9327 (1997).
[7] S. S. Sarman, D. J. Evans, and P. T. Cummings, Physics Reports—Review Section of Physics Letters **305**, 1 (1998); C. McCabe, D. Bedrov, G. D. Smith, and P. T. Cummings, Ind. Eng. Chem. Res. **40**, 473 (2001); C. McCabe, C. W. Manke, and P. T. Cummings, J. Chem. Phys. **116**, 3339 (2002).
[8] C. McCabe, S. T. Cui, and P. T. Cummings, Fluid Phase Equilib. **183**, 363 (2001).

[9] C. McCabe, S. T. Cui, P. T. Cummings, P. A. Gordon, and R. B. Saeger, J. Chem. Phys. **114**, 1887 (2001).
[10] D. J. Evans and G. P. Morriss, Phys. Rev. A **30**, 1528 (1984).
[11] D. J. Evans and G. P. Morriss, *Statistical Mechanics of Nonequilibrium Liquids* (Academic, New York, 1990).
[12] G. P. Morriss and D. J. Evans, Phys. Rev. A **35**, 792 (1987).
[13] D. J. Evans and G. P. Morriss, Phys. Rev. A **38**, 4144 (1988).
[14] I. Borzsak, P. T. Cummings, and D. J. Evans, Mol. Phys. **100**, 2735 (2002).
[15] J. Delhommelle and P. T. Cummings, Phys. Rev. B **72**, 172201 (2005).
[16] J. W. Dufty and M. J. Lindenfeld, J. Stat. Phys. **20**, 259 (1979).
[17] M. E. Tuckerman, C. J. Mundy, and G. J. Martyna, Europhys. Lett. **45**, 149 (1999).
[18] S. Nosé, J. Chem. Phys. **81**, 511 (1984).
[19] K. P. Travis, P. J. Daivis, and D. J. Evans, J. Chem. Phys. **103**, 1109 (1995).
[20] K. P. Travis, P. J. Daivis, and D. J. Evans, J. Chem. Phys. **103**, 10638 (1995); J. Chem. Phys. **105**, 3893 (1996).
[21] L. Lue, O. G. Jepps, J. Delhommelle, and D. J. Evans, Mol. Phys. **100**, 2387 (2002).
[22] F. Zhang, J. Chem. Phys. **106**, 6102 (1997).
[23] G. A. Pan, J. F. Ely, C. McCabe, and D. J. Isbister, J. Chem. Phys. **122**, 4114 (2005).
[24] M. E. Tuckerman, B. J. Berne, and G. J. Martyna, J. Chem. Phys. **97**, 1990 (1992).
[25] M. Watanabe and M. Karplus, J. Chem. Phys. **99**, 8063 (1993); L. I. Kioupis and E. J. Maginn, Chem. Eng. J. **74**, 129 (1999).
[26] C. J. Mundy, J. I. Siepmann, and M. L. Klein, J. Chem. Phys. **102**, 3376 (1994).
[27] S. T. Cui, P. T. Cummings, and H. D. Cochran, J. Chem. Phys. **104**, 255 (1996).
[28] J. I. Siepmann, S. Karaborni, and B. Smit, J. Am. Chem. Soc. **115**, 6454 (1993).
[29] W. L. Jorgensen, J. D. Madura, and C. J. Swenson, J. Am. Chem. Soc. **106**, 6638 (1984).
[30] C. J. Mundy, J. I. Siepmann, and M. L. Klein, J. Chem. Phys. **102**, 3376 (1995).
[31] S. T. Cui, P. T. Cummings, and H. D. Cochran, Mol. Phys. **88**, 1657 (1996).
[32] B. D. Todd, Phys. Rev. E **58**, 4587 (1998).
[33] M. M. Cross, J. Colloid Sci. **20**, 417 (1965).
[34] G. Ciccotti and J. P. Ryckaert, Comput. Phys. Rep. **4**, 345 (1986); R. L. C. Akkermans and W. J. Briels, J. Chem. Phys. **114**, 1020 (2001); W. K. den Otter, M. Krohn, and J. H. R. Clarke, Phys. Rev. E **65**, 016704 (2002); R. L. C. Akkermans and G. Ciccotti, J. Phys. Chem. B **108**, 6866 (2004); G. Marechal and J. P. Ryckaert, Chem. Phys. Lett. **101**, 548 (1983); M. P. Allen, Mol. Phys. **52**, 717 (1984).